processes

MDPI

Article

Analysis and Optimization of Thermal Storage Performance of Thermocline Storage Tank with Different Water Distribution Structures

Xinwei Wang [1,*], Longbin Duan [1], Genying Gao [2], Weibo Zheng [1,3], Dong Sun [3], Jinyu Li [1], Jing Fu [1] and Riyi Lin [1]

[1] College of New Energy, China University of Petroleum (East China), Qingdao 266580, China; duanlb179@163.com (L.D.); zhengweibo.slyt@sinopec.com (W.Z.); lijinyu1525@163.com (J.L.); fujing5642@163.com (J.F.); linry@upc.edu.cn (R.L.)
[2] Oil Production Technology Research Institute, China National Petroleum Corp. Xinjiang Oil Field, Karamay 834000, China; gaogy2@petrochina.com.cn
[3] Shengli Oilfield Technical Inspection Center, SlNOPEC, Dongying 257000, China; sundong.slyt@sinopec.com
* Correspondence: wangxw@upc.edu.cn; Tel.: +86-0532-8698-1771

Abstract: Energy storage is essential for solar energy utilization, and thermocline storage tanks are commonly used. To improve temperature stratification and storage efficiency, we investigated the effect of different water distributor configurations on tank stratification. We numerically analyzed the heat storage processes in hot water tanks with three water distribution configurations: star, antenna, and octagonal. Temperature stratification was evaluated based on thermocline thickness and storage efficiency. Thermal storage efficiency improves by 0.45% when the outlet direction of the water distributor matches the fluid's motion direction during natural stratification. The energy storage process is categorized into three stages based on efficiency changes, with different factors affecting efficiency at each stage. In the initial stage, antenna-type and octagonal water distribution improve temperature uniformity along the axial section, reduce thermocline thickness, and enhance stratification. Final efficiency during this stage is primarily influenced by energy loss resulting from the mixing of hot and cold water. In the development stage, energy storage efficiency decreases mainly because the lower boundary of the thermocline reaches the exit, causing partial discharge of hot water. Among the three configurations, the octagonal water distribution exhibits the lowest energy loss, 6.4% lower than that of the star-type distribution.

Keywords: energy storage; thermocline storage tank; thermocline thickness; water distribution structure

check for updates

Academic Editor: Kian Jon Chua

Received: 26 January 2025
Revised: 14 February 2025
Accepted: 21 February 2025
Published: 22 February 2025

Citation: Wang, X.; Duan, L.; Gao, G.; Zheng, W.; Sun, D.; Li, J.; Fu, J.; Lin, R. Analysis and Optimization of Thermal Storage Performance of Thermocline Storage Tank with Different Water Distribution Structures. *Processes* **2025**, *13*, 629. https://doi.org/10.3390/pr13030629

Copyright: © 2025 by the authors. Licensee MDPI, Basel, Switzerland. This article is an open access article distributed under the terms and conditions of the Creative Commons Attribution (CC BY) license (https://creativecommons.org/licenses/by/4.0/).

1. Introduction

Aligning energy transition with sustainable development goals necessitates the swift adoption of renewable energy across various sectors with high energy demand [1,2]. Recently, with rising energy consumption and increased oil extraction, oil reservoirs have moved into secondary and tertiary recovery stages. This shift has intensified fossil fuel consumption during extraction and refining, exacerbating the mismatch between peak and off-peak power loads [3]. Consequently, oilfield companies and researchers are exploring more efficient and environmentally friendly methods to stabilize oil production [4,5]. Simultaneously, to transform the energy utilization structure and enhance the use of renewable energy in oilfield operations, the concept of the "Energy Internet" has been introduced [6,7]. This approach aims to integrate waste heat from the oilfield pipeline network, renewable

energy sources, grid power supply, energy storage systems, and regional heat users into a cohesive and manageable system.

In the "Energy Internet", the energy storage system is crucial for storing energy provided by the energy supply system and transferring it to heat users to meet their heat demand through energy release, where the energy is primarily stored in the form of heat. TCST offers advantages such as safety, high efficiency, ease of operation, and cost-effectiveness, and is widely implemented in thermal energy storage systems [8,9]. According to the number of heat storage tanks, the TCST system can be classified into double-tank and single-tank heat storage systems. Although the double-tank heat storage system effectively reduces the mixing of hot and cold fluids, the average heat storage cost of the single-tank heat storage system is significantly lower than that of the double-tank system, making it more prevalent in practical applications [10]. Figure 1 illustrates the schematic diagram of the single-tank heat storage system frequently employed in oil fields. Inside the heat storage tank, hot water with lower density occupies the upper part of the tank, while cooler water with higher density settles in the lower part. This density difference results in natural stratification within the tank, creating a temperature gradient known as the thermocline [11]. Hot water is injected or extracted from the upper part of the storage tank, while cold water is extracted or injected from the lower part during the heat storage process or the heat release process.

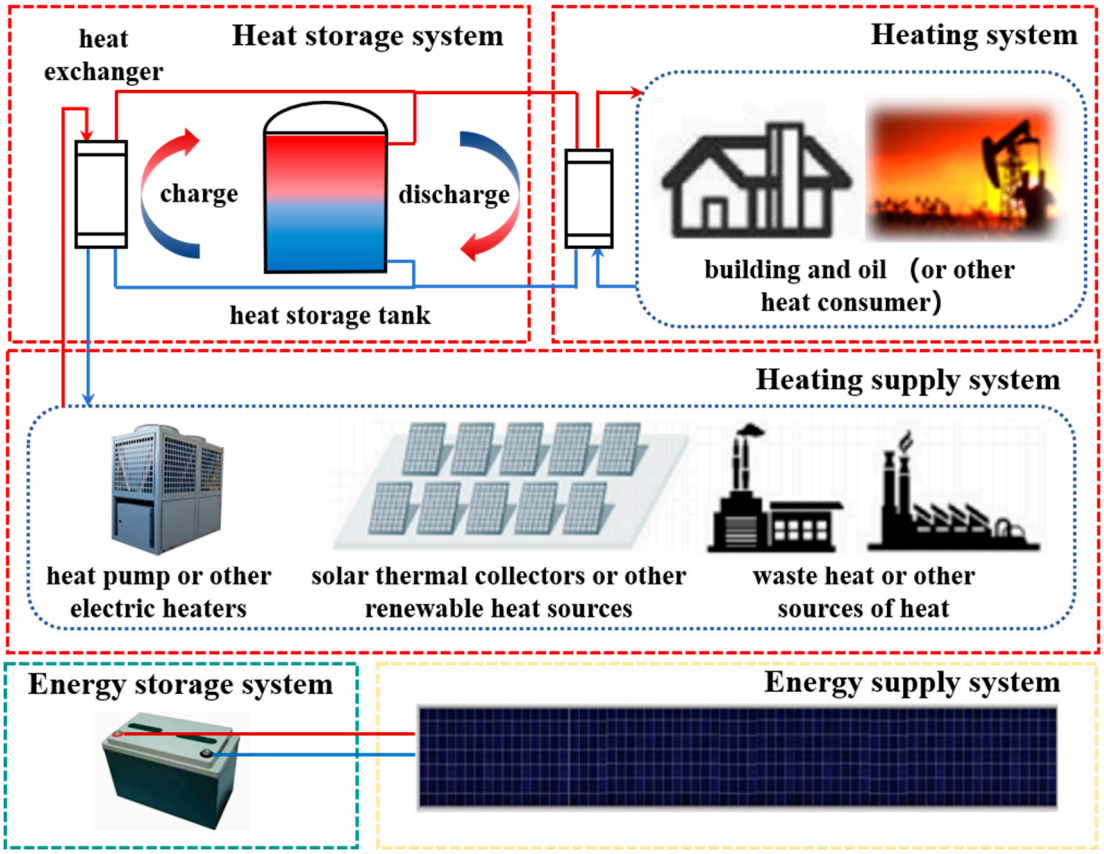


Figure 1. Schematic diagram of thermocline thermal storage tank system.

Thermocline will have an important impact on the performance of the storage tank. It will vary with the tank's shape, water distribution structure, inlet flow rate, and the times of heat storage and release. Studies have shown that reducing the volume of the thermocline region in the tank can significantly enhance the heat storage and release efficiency of the thermocline storage system [12]. Therefore, to reduce the thickness of

the thermocline, researchers have extensively studied the thermocline's evolution [13], fluid flow and heat transfer characteristics, and variations in energy and exergy within tanks under various conditions using experimental and numerical simulation methods [14]. The tank's geometry and height-to-diameter ratio are key factors affecting thermocline characteristics. Chen et al. investigated fluid distribution and temperature stratification in heat storage tanks using numerical simulations and experiments. Their results indicated that the tank's geometry influences fluid flow and heat transfer processes [15]. Li examined the variation of the thermocline in cylindrical tanks with different height-to-diameter ratios while maintaining a constant radius using numerical simulations. It was found that a larger height-to-diameter ratio increases temperature stratification in the tank [16]. Ievers et al. proposed that the optimal height-to-diameter ratio for cylindrical storage tanks is 3.5, balancing economic and practical considerations. They noted that exceeding this ratio does not significantly improve stratification effects and increases construction costs [17]. Yang et al. assessed the energy storage efficiency of ten types of energy storage tanks with varying structures using numerical simulations. Their findings indicate that the specific surface area is the primary determinant of energy storage efficiency. Spherical and barrel structures are identified as the most efficient, while cylindrical structures exhibit the lowest efficiency [14]. Khurana et al. employed a 2D model to analyze the stratification characteristics of energy storage tanks with conical, parabolic, and cylindrical surfaces. They found that increasing the height-to-diameter ratio of conical and parabolic tanks deteriorates temperature stratification and results in greater energy losses [18].

The operational parameters of the thermocline thermal storage system significantly affect the thermocline within the tank. Li investigated the impact of parameters such as mass flow rate and fluid properties on storage efficiency through numerical simulations. The study shows that stratification is poor at low flow rates, though increasing the flow rate enhances stratification. However, higher flow rates also increase fluid mixing, creating a trade-off between heat transfer and heat diffusion, resulting in an optimal mass flow rate [16]. Wang et al. employed the Richardson number and the MIX number to analyze exergy efficiency. As the flow rate increases, the Richardson number decreases, and efficiency initially increases before subsequently decreasing [19]. Dragsted et al. conducted top storage experiments and examined energy changes in different horizontal stratifications of the hot water storage tank, with water distribution arranged vertically, using the MIX number. Increased flow rates lead to greater energy losses in the upper part of the tank [20]. Rahman et al. investigated the effects of flow rate and transient heat sources on temperature distribution within the heat storage tank. When the injection temperature varies sinusoidally, there is a lag in the temperature change of the stored water [21]. The impact of temperature changes on the thermocline varies significantly with working conditions, leading to different conclusions among scholars. Yaïci et al. found through numerical simulations that variations in inlet and outlet temperatures have minimal impact on the formation and development of the thermocline [22]. Nelson et al. found that an increased temperature difference between the inlet and outlet enhances the degree of stratification inside the tank [23]. Shaikh et al. demonstrated that an increased temperature difference between the inlet and outlet, as reflected by the Atwood number, enhances stratification. As the temperature difference between hot and cold water increases, buoyancy becomes the dominant factor in thermocline formation, and the thickness of the thermocline increases with the Atwood number [24]. Additionally, as heat dissipation to the surroundings occurs during energy storage, a larger temperature difference between the inlet and outlet increases the impact of heat loss on temperature stratification within the tank [23,25]. Consequently, variations in the temperature difference between the inlet and outlet affect temperature stratification differently.

By installing water distributors and baffles at both the inlet and outlet, the fluid flow and heat transfer characteristics within the energy storage tank can be modulated. This influences the thermocline thickness and energy storage efficiency, leading to extensive research on optimizing these components. Luo et al. employed numerical simulations and experimental methods to investigate the heat storage process in energy storage tanks equipped with ring-opening plate distributors (ROPDs). This study aimed to optimize the thermal storage process of energy storage tanks by adjusting the opening size of the water distributor, reducing thermal jet perturbations, and mitigating the efficiency decline when the Reynolds number in the tank exceeds 167 ($Re_{tank} > 167$) [10]. Xu et al. analyzed cylindrical water tanks with various heat insulation panel structures through numerical simulations. The thickness and thermal conductivity of these panels were found to affect exergy efficiency and stability during heat storage and discharge. Increasing the insulation panel thickness while decreasing thermal conductivity improved performance [26]. Gao et al. investigated the impact of center-open refractory plates on fluid flow and temperature distribution in cylindrical energy storage tanks using both experiments and numerical simulations. Optimal structural parameters were determined through structure optimization based on the Richardson number [27]. Karim determined the optimal structural parameters by experimentally studying fluid mixing in energy storage tanks with octagonal water distributors under various operating conditions. The design and layout of the diffuser significantly affect mixing near the inlet diffuser, and this mixing plays a crucial role in the development of the thermocline [28]. Hosseinnia et al. categorized the development of the thermocline into three stages, noting that parallel disk water distributors can mitigate momentum perturbations and reduce the slant temperature thickness [29]. Chung et al. studied thermocline development in cylindrical energy storage tanks using the Richardson number and identified optimal structural parameters. Their numerical simulations of tanks with three water distribution types—radial, adjustable plate, and H-type—showed that the inlet Reynolds number had a more pronounced effect on stratification compared to the Froude number [30]. In conclusion, optimizing the water distribution structure is crucial for enhancing energy storage efficiency and improving the stratification of the energy storage tank.

In previous studies examining the impact of the installation of water distributors and baffles on the energy storage efficiency of thermal storage tanks, the primary focus has been on the influence of dimensionless numbers such as Reynolds number and Froude number on storage efficiency during the energy storage process. However, these studies overlooked the effects of structural parameter changes on flow distribution and the uniformity of the temperature within the tank, as well as the changes in heat transfer characteristics within the tank caused by the aforementioned factors. In this study, we focus on investigating the influence of different structural designs of water distributors on flow distribution and temperature uniformity. We explore the impact of temperature non-uniformity on heat conduction within the tank and the storage efficiency, and conduct structural optimization of the water distributor. Additionally, in studies such as those by Luo et al. [10], Li [16], and others, the working conditions primarily involve low Reynolds numbers, with limited research on high Reynolds number conditions. In contrast, Tang et al. explored the design of an octagonal water distributor in large-flow energy storage systems, which proved to be relatively complex [31]. In our work, we simplify the design of the octagonal water distributor under high Reynolds number conditions and optimize its selection for high-flow, high-Reynolds-number scenarios.

In the oilfield TCST system shown in Figure 1, the energy storage tank typically has a small height-to-diameter ratio, and experiences a high Reynolds number during the heat storage and release process. This study designs three water distribution structures:

star-type, octagonal-type, and antenna-type, and conducts 3D numerical simulations using the computational fluid dynamics software ANSYS Fluent 2021 R1(Pennsylvania, US). The simulations assess the impact of different water distribution methods and structures on the energy storage efficiency and stratification in the TCST system. The study further simulates the thermocline energy storage system with various water distribution installations to evaluate the energy storage efficiency and stratification during heat storage and discharge processes. The findings provide guidance for selecting and optimizing water distributor installations, structures, and hole arrangements, and help determine the most suitable water distributor structure for thermocline heat storage systems with a small height-to-diameter ratio and high Reynolds number.

2. Numerical Modelling

2.1. Geometry Description

In this paper, a heat storage water tank with a diameter (R) of 2.2 m and an effective height (H) of 1.5 m is used as the research focus. The tank is equipped with upper and lower water distributors installed at 0.05 m from both the top and bottom, respectively, disregarding the effect of the air layer at the top of the arched tank on its thermal performance. The final simplified physical model is shown in Figure 2, where R is the radius of the tank, δ_1 is the wall thickness, δ_2 is the thickness of the thermocline, H is the effective height, T_w is the temperature of the water in the tank, h_w is the convective heat transfer coefficient between the water and the inner wall of the tank, T_∞ is the ambient temperature, and h_∞ is the convective heat transfer coefficient between the air and the outer wall of the tank.

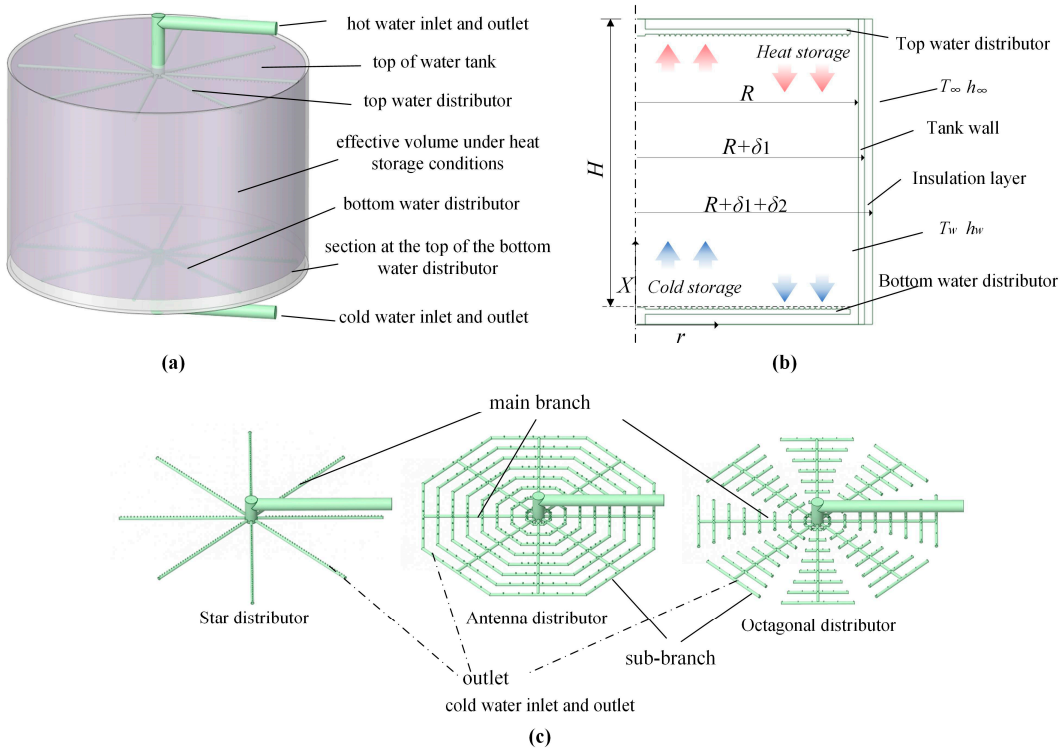


Figure 2. Geometry and dimensions of the cylindrical storage tank equipped with water distributor. (**a**) Overall appearance structure; (**b**) vertical cross-section; (**c**) Structure of water distributor.

When the tank is in the storage and exothermic process, the average temperature of the water in the tank changes from the initial temperature to the injection temperature with minimal fluctuations. Therefore, the arithmetic mean of the temperatures of the hot and cold water during these processes is used as the qualitative temperature of the

water in the tank, T_w. All subsequent calculations use the physical parameters of the water corresponding to this qualitative temperature. The tank's exterior is insulated with high-foam polyethylene material, approximately 30 mm thick, with a thermal conductivity 0.043~0.056 W/(m·K). To simplify heat dissipation calculations, the thermal effects of the stainless steel outer wall, the thermocline, and the external environment on the working mass inside the tank are combined into a single convective heat transfer coefficient, h. The heat exchange between the air and the thermocline is considered a self-consistent convective heat transfer. The total convective heat transfer coefficient is calculated using the multilayer cylindrical wall model as specified in Equations (1)–(3).

$$\Phi = \frac{A(T_w - T_\infty)}{\frac{1}{h_w R} + \frac{\ln\left[\frac{R+\delta_1}{R}\right]}{\lambda_1} + \frac{\ln\left[\frac{R+\delta_1+\delta_2}{R+\delta_1}\right]}{\lambda_2}} \tag{1}$$

$$\Phi = Ah(T_w - T_\infty) \tag{2}$$

$$A = 2\pi RH \tag{3}$$

where λ_1 is the thermal conductivity of the stainless steel wall of the heat storage tank, W/(m·K), and λ_2 is the thermal conductivity of the insulation material, W/(m·K).

The physical significance and value of each parameter in the calculation process are shown in Table 1.

Table 1. Value of calculation parameters.

Parameter	Value
H/(mm)	1500
R/(mm)	1100
δ_1/(mm)	10
δ_2/(mm)	30
λ_1/W/(m·K)	16.2
λ_2/W/(m·K)	0.05
T_w/(°C)	75
T_∞/(°C)	23
h_w/W/(m·K)	200
h_∞/W/(m·K)	8

The total convective heat transfer coefficient h = 9.69 W/(m·K) in this study.

In the heat storage process, hot water is introduced into the tank through an upper distribution, which facilitates the formation of a thermocline near the upper region of the tank. The flow of cold water, exiting through the lower distribution, tends to be more uniform, with a relatively slower average flow rate within the tank. Consequently, it is deemed that the lower distribution has a negligible effect on the overall storage efficiency. Therefore, the influence of the lower water distribution on storage efficiency is considered minimal and is not included in detailed analyses. Instead, studies on the heat storage process focus on the effective volume, which is defined as the cross-sectional area from the top of the tank to the outlet of the upper water distribution.

The average flow velocity at the outlet of the water distributor can be calculated using Equation (4),

$$\overline{v_{in}} = \frac{q_v}{\pi n r^2} \tag{4}$$

where q_v is the volumetric flow rate in m^3/s, n is the number of outlets of the water distributor, and r is the outlet radius in meters.

2.2. Governing Equations

The control equation is shown below:

Continuity equation:

$$\frac{\partial(\rho u)}{\partial x} + \frac{\partial(\rho v)}{\partial y} + \frac{\partial(\rho w)}{\partial z} = 0 \tag{5}$$

Energy equation:

$$\rho\left(\frac{\partial T}{\partial t} + u\frac{\partial T}{\partial x} + v\frac{\partial T}{\partial y} + w\frac{\partial T}{\partial z}\right) - \rho T\left(\frac{\partial u}{\partial x} + \frac{\partial v}{\partial y} + \frac{\partial w}{\partial z}\right) = \frac{k}{c_p}\left(\frac{\partial^2 T}{\partial x^2} + \frac{\partial^2 T}{\partial y^2} + \frac{\partial^2 T}{\partial z^2}\right) \tag{6}$$

Momentum equation:

$$\begin{aligned}
\rho\left(\tfrac{\partial u}{\partial t} + u\tfrac{\partial u}{\partial x} + v\tfrac{\partial u}{\partial y} + w\tfrac{\partial u}{\partial z}\right) &= \mu\left(\tfrac{\partial^2 u}{\partial x^2} + \tfrac{\partial^2 u}{\partial y^2} + \tfrac{\partial^2 u}{\partial z^2}\right) - \tfrac{\partial P}{\partial x} \\
\rho\left(\tfrac{\partial v}{\partial t} + u\tfrac{\partial v}{\partial x} + v\tfrac{\partial v}{\partial y} + w\tfrac{\partial v}{\partial z}\right) &= \mu\left(\tfrac{\partial^2 v}{\partial x^2} + \tfrac{\partial^2 v}{\partial y^2} + \tfrac{\partial^2 v}{\partial z^2}\right) - \tfrac{\partial P}{\partial y} + \rho g \\
\rho\left(\tfrac{\partial w}{\partial t} + u\tfrac{\partial w}{\partial x} + v\tfrac{\partial w}{\partial y} + w\tfrac{\partial w}{\partial z}\right) &= \mu\left(\tfrac{\partial^2 w}{\partial x^2} + \tfrac{\partial^2 w}{\partial y^2} + \tfrac{\partial^2 w}{\partial z^2}\right) - \tfrac{\partial P}{\partial z}
\end{aligned} \tag{7}$$

where ρ is water density. c_p is specific heat capacity. k is thermal conductivity of water.

In order to study the effect of thermal insulation performance on the energy storage efficiency of the heat storage water tank, the side wall surfaces of the tank are modeled with the third type of boundary conditions, with the heat transfer coefficient set as the total heat transfer coefficient calculated in Section 2.1, while the remaining wall surfaces are modeled as adiabatic. The temperature of the hot water during storage and release conditions is 363.15 K, while the temperature of the cold water is 333.15 K. The inlet type is specified as velocity inlet, and the inlet position and flow rate are adjusted based on different studies. The outlet type is specified as outflow. Due to the turbulence at the outlet of the water distributor, the standard k-ε model is employed, and the wall function utilizes the enhanced wall treatment. During the calculation, the physical parameters of the water, except for density, remain constant with temperature. The Boussinesq model is used to account for the temperature-dependent variation in water density. The computational model and discretization settings are presented in Table 2. The convergence criteria for the residuals of the continuity and momentum equations are set to 10^{-3}, while the convergence criteria for the residuals of the energy equation are set to 10^{-6}.

Table 2. The calculated model and related parameter settings used.

Model Parameter	Setting
Pressure–velocity coupling scheme	PISO
Pressure discretization Momentum discretization Energy discretization Turbulent kinetic energy discretization Turbulent Dissipation discretization	Second order upwind

2.3. Parameter Dimensionless

Differences in fluid temperatures result in density variations, and stratification occurs under the influence of gravity: lower-temperature fluids are denser and positioned below, while higher-temperature fluids are less dense and positioned above. When the temperature of the fluid in the tank is stabilized, a temperature gradient region is created, referred to as the thermocline. The presence of the thermocline prevents the mixing of hot and cold fluids. The greater the thickness of the thermocline, the less heat is transferred from the high-temperature fluid to the low-temperature fluid region, complicating heat storage in

the high-temperature fluid region and resulting in a reduction in the thermal efficiency of the energy storage tank.

Usually used to define the dimensionless temperature to determine the thermocline region, the expression is shown in Equation (8):

$$\theta = (T_{ms} - T_c)/(T_h - T_c) \tag{8}$$

where T_{ms} is the temperature of a fluid at a certain location, T_c represents the cold water temperature, which is 333.15 K in this paper, and T_h represents the hot water temperature, which is 363.15 K in this paper.

The thickness of the thermocline is calculated as shown in Equation (9):

$$\delta = \begin{cases} H_{\text{crit},h} - H_{\text{crit},l} & \left(T_{\text{bottom}} \le T_{\text{crit},l}, T_{\text{top}} \ge T_{\text{crit},h}\right) \\ H_{\text{crit},h} - H_{\text{bottom}} & \left(T_{\text{bottom}} > T_{\text{crit},l}\right) \\ H_{\text{top}} - H_{\text{crit},l} & \left(T_{\text{top}} < T_{\text{crit},h}\right) \end{cases} \tag{9}$$

where δ is the thickness of the thermocline, $T_{\text{crit},l}$ is the lowest fluid temperature of the thermocline (θ = 0.05), $H_{\text{crit},l}$ is the location of the lowest fluid temperature of the thermocline, $T_{\text{crit},h}$ is the highest fluid temperature of the thermocline (θ = 0.95), and $H_{\text{crit},h}$ is the location of the highest fluid temperature of the thermocline. T_{top} and T_{bottom} are the fluid temperatures at the top and bottom of the storage tanks, respectively, and H_{top} and H_{bottom} denote the locations at the top and bottom of the storage tanks. $H_{\text{crit},h}$ is the location of the highest fluid temperature in the inclined thermocline. The same values of $T_{\text{crit},l}$ and $T_{\text{crit},h}$ are used to calculate the thickness of the sloped thermocline for the same set of comparison conditions at the same moment.

Due to the different working conditions, the tank structure of the effective height of the tank is different, the dimensionless thermocline thickness can reflect the volume share of the thermocline in the tank, and the dimensionless thermocline thickness δ^* is calculated as shown in Equation (10):

$$\delta^* = \frac{\delta}{H} \tag{10}$$

The dimensionless time τ* is the time scale reflecting the progress of heat storage and heat release in the heat storage tank, which is calculated as shown in Equations (11) and (12):

$$\tau_e = \frac{V}{q_v} \tag{11}$$

$$\tau^* = \frac{\tau}{\tau^e} \tag{12}$$

where τ_e is the time required for one complete rotation of cold or hot water, s, V is the tank volume, m^3, q_v is the mass flow rate, m^3/s, τ^* is the dimensionless time, and τ is the energy storage time, s.

When τ^* = 1, the hot water in the heat storage process completely displaces the cold water in the tank in the case of complete stratification of hot and cold water in the tank.

The inlet Reynolds number and the tank Reynolds number can be calculated by Equations (13) and (14)

$$Re_{in} = \frac{\rho \overline{v_{in}} d}{\mu} \tag{13}$$

$$Re_{tank} = \frac{\rho \overline{v_{tank}} D}{\mu} \tag{14}$$

where D is the diameter of the tank, d is the diameter of the water distributor outlet, and for convenience in calculations, ρ, μ is taken as the value for water at 333.15 K.

The bulk Froude number (Fr) is calculated by Equation (15) [10]:

$$Fr = \frac{\overline{v}_{in}}{[dg(\rho_c - \rho_h)/\rho_c]^{1/2}} \tag{15}$$

where ρ_c is the density of cold fluid at 333.15 K, ρ_h is the density of hot fluid and g is the gravitational acceleration.

2.4. Energy Storage Efficiency

In addition to the thickness of the thermocline, energy storage efficiency is a crucial metric for assessing the performance of an energy storage tank. Typically, an efficient energy storage tank has an energy storage efficiency of 85% or higher. Energy storage efficiency (η) is defined as the ratio of the actual amount of heat (or cold) stored in the tank to the theoretical maximum amount of heat (or cold) that the tank could store. This coefficient takes into account various factors such as heat loss due to the mixing of hot and cold water, heat conduction within the thermocline region, and convective heat transfer losses to the tank walls and the external environment. Hence, it serves as a key indicator of the tank's efficiency in storing energy. The calculation is shown in Equations (16)–(18).

$$\eta = \frac{Q_{act}}{Q_{the}} \tag{16}$$

$$Q_{the} = \int_0^{\tau_e} c\rho q_v (T_{in} - T_{out}) dt \tag{17}$$

$$Q_{act} = \int_0^{\tau_e} c\rho q_v (T'_{in} - T'_{out}) - Ah(\overline{T}_{wall} - T_\infty) dt \tag{18}$$

where Q_{the} is the theoretical heat (cold) storage volume, Q_{act} is the actual heat (cold) storage volume, τ_e is the time required for injecting the volume of hot (cold) water into the effective volume of the tank, q_v is the volumetric flow rate of the main circuit of the water distributor, T_{in} is the theoretical inlet temperature, T_{out} is the theoretical tank outlet temperature, $T_{in'}$ is the actual inlet temperature, $T_{out'}$ is the actual tank outlet temperature, and $\overline{T}_{wall}$ is the average tank sidewall surface temperature.

2.5. Grid Independence Analysis

In order to verify the independence of the grid and the time step, the mesh function in Workbench was used for meshing in this study. By adjusting the mesh size, three different mesh counts were obtained: 7,127,731, 4,830,715, and 2,582,587. Figure 3 illustrates the variation in the average temperature inside the tank during the heat storage process. The phase error is more significant between the mesh counts of 4,830,715 and 2,582,587. Additionally, the temperature distribution differences are smaller when the mesh count exceeds 4,830,715. The accuracy of the numerical results does not improve with an increasing number of cells. However, computation time increases. Therefore, to enhance computational efficiency, a mesh count of 4,830,715 and a time step of 0.2 s were chosen for this study.

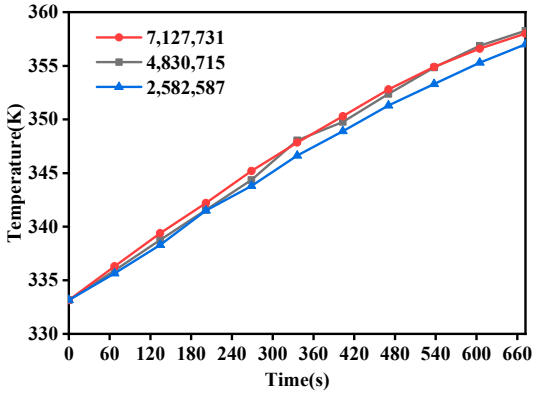


Figure 3. Model validation.

To ensure the accuracy of the model parameter settings, a rationality verification is required before the simulation begins to ensure alignment with actual conditions. A physical model of the tank is established based on the tank used in Karim's experiment [31], and the same simulation parameters are adopted for the simulation. The tank is made of 10mm glass fiber, with a height of 1850 mm and a diameter of 850 mm. The distributor has an octagonal structure, installed 25 mm above the bottom, with four opening holes in each arm, providing a total opening area of 45 cm^2. The octagons are formed by eight straight sections, each 23.8 cm long, connected by 45° elbows. The initial temperature inside the tank is 5 °C, the inlet water temperature is 17 °C, and the flow rate is 8 L/min. After running for 100 min, the temperature distribution curve along the centerline of the tank is plotted and compared with experimental results (Figure 4) to verify the rationality of the model parameter settings.

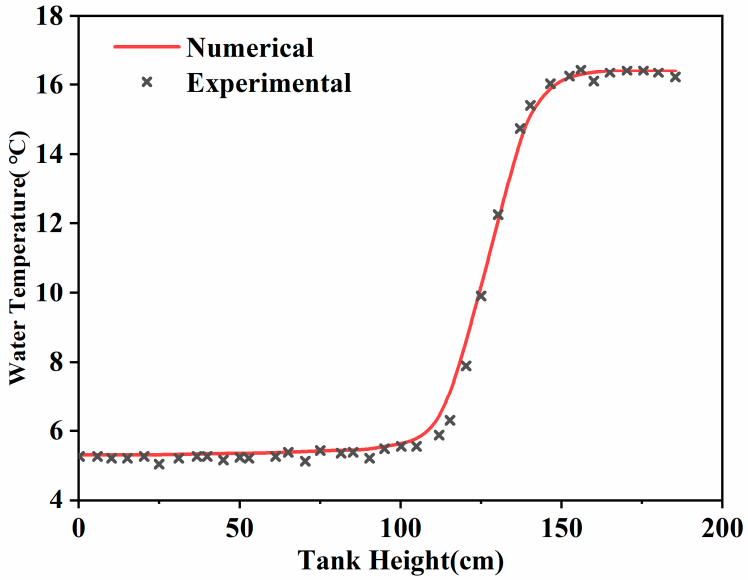


Figure 4. Comparison of experimental and numerical.

The comparison reveals that the temperature distribution trend along the centerline in both the simulation and experiment is similar, with temperature values being fairly close. However, there is a certain degree of discrepancy between the simulation and experimental values at the top and bottom of the tank. This is primarily due to the assumption of an adiabatic tank and inlet/outlet pipe walls in the simulation, which creates relatively idealized boundary conditions, whereas the experiment cannot achieve a completely adiabatic condition. Additionally, the arrangement of thermocouples in the

experiment introduces disturbances, and measurement errors from the thermocouples may contribute to deviations. By comparing the experimental results and numerical simulation results shown in the figure, the maximum temperature difference between the experiment and simulation is found to be 0.9 K, with the maximum error calculated to be 5.7%. It is concluded that the results from both the experiment and numerical simulation are relatively reliable.

3. Calculation Results and Discussion

3.1. Influence of the Direction of Installation of the Water Distributor on the Effectiveness of Heat Storage

In the process of energy storage, the direction of the water distribution outlet determines the flow direction of the injected water in the tank. In the initial stage, the mixing of hot and cold fluids in the tank primarily occurs near the outlet of the water distribution. At this stage, the inertia force at the outlet and the buoyancy force in the adjacent area jointly determine the formation of a thermocline, including its thickness. Subsequently, changes in the thickness of the thermocline affect the efficiency of energy storage.

To exclude the effects of uneven distribution at the water distributor outlets, we assume a star-type water distributor with an outlet flow rate equal to the inlet flow rate of 30.52 m^3/h (Re_{in} = 6984). Numerical simulations are performed for heat storage conditions with the upper water distributor outlet directed both vertically upward and downward, and for cold storage conditions with the lower water distributor outlet also directed both vertically upward and downward. The distributor has 288 holes, each 5 mm in diameter. For convenience, these four conditions are labeled as Case 1–Case 4. The temperature distributions on the center-axis surface for these conditions, when τ^* = 0.4, are shown in Figures 5 and 6.

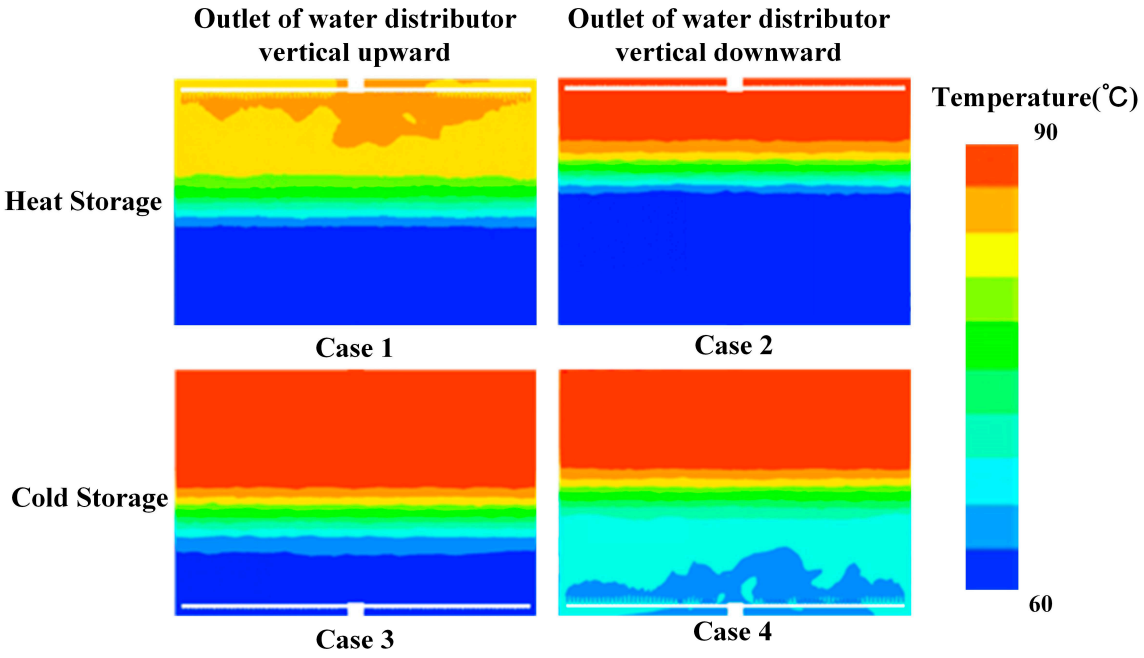


Figure 5. Temperature field diagram of thermal storage tank under charging and discharging conditions.

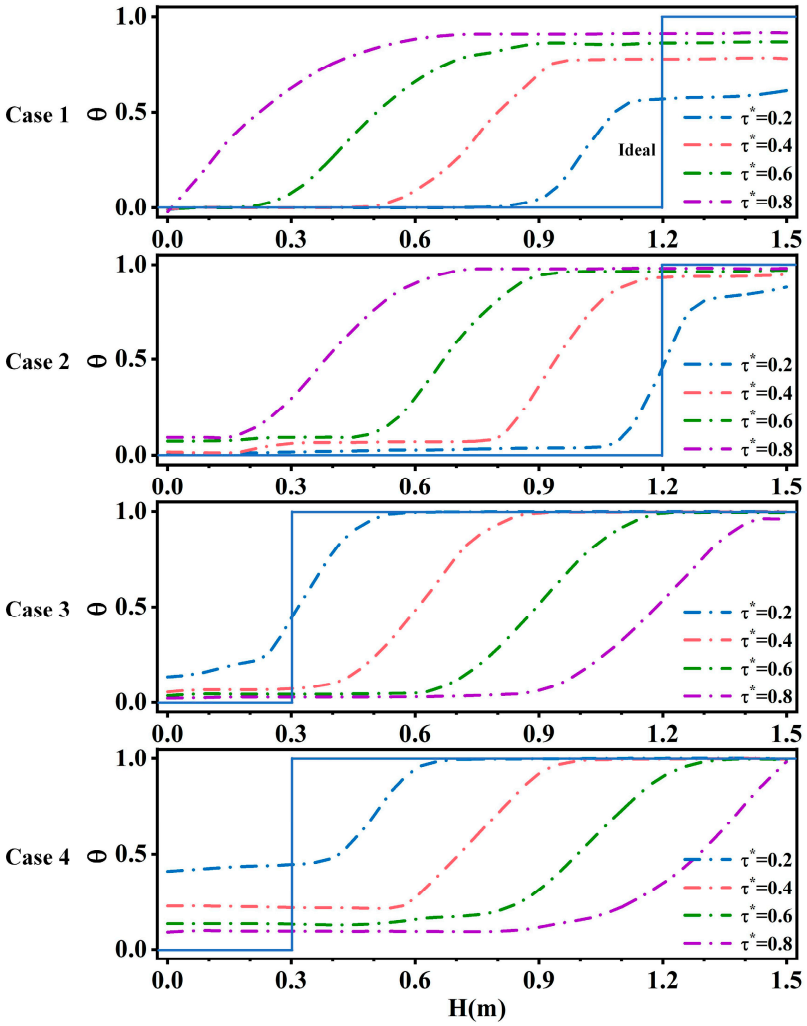


Figure 6. The variation of dimensionless temperature δ^* with dimensionless time τ^*.

From Figures 5 and 6, it can be observed that during the heat storage process, at the upper water distributor outlet, where cold water and injected hot water mix, the density of temperature increase decreases. Due to buoyancy, the hot water rises to the upper part of the tank. When the outlet is downward, the injected hot water experiences downward inertial forces and mixes with the upward-moving heated cold water, impeding the upward movement and inhibiting the formation of a thermocline. Consequently, a mixing region forms near the outlet, where the temperature is lower than the inlet. The regional average temperature increases gradually with the injection of hot water during heat storage. A mixing region forms near the outlet, where the average temperature is lower than the injected hot water temperature. As the hot water injection process continues, a vigorous mixing of hot and cold water occurs, causing the average temperature to gradually increase as hot water is injected into the thermal storage process. Due to the inertia of the hot water moving downward, the forced convection enhances the axial heat transfer within the tank. In the same axial interface at the same time, the area occupied by cold fluid is smaller, and the duration of the calm cold environment in the middle region is shorter. Conversely, when the outlet is upward, the direction of hot water injection aligns with the flow direction of the heated cold water, resulting in a high-temperature zone at the top of the tank where the temperature of the export hot water is similar. This configuration leads to a thinner thermocline slope between the hot and cold water.

In Figure 6, the temperature distribution at $\tau^* = 0.2$ representing complete stratification was added, providing a comparison between ideal and actual operation. By comparing with the temperature distribution under complete stratification, the degree of stratification can be inferred. The temperature distributions in Case 2 and Case 3 are closer to the distribution at complete stratification within the tank, showing more pronounced stratification. Additionally, the temperature curve has a steeper slope, and the thickness of the stratified layer is smaller. Under ideal operating conditions, the outlet temperature only begins to change after $\tau^* = 1$. Prior to this moment, the outlet water remains unblended, thus preventing any energy loss. The average temperature of the outlet of the energy storage tank varies with time as shown in Figure 7. The outlet temperature undergoes significant changes at $\tau^* = 0.7$ during both the heat and cold storage processes. In the heat storage process, when the water distributor outlet is oriented downward, axial heat transfer of the hot water is enhanced, the formation of the thermocline becomes thicker, and the distance between the thermocline boundary and the tank outlet is reduced. In comparison to when the outlet is oriented upward, the temperature at the cold water outlet changes earlier, and more heated water is simultaneously discharged with the cold water. This leads to energy wastage and reduced efficiency of energy storage.

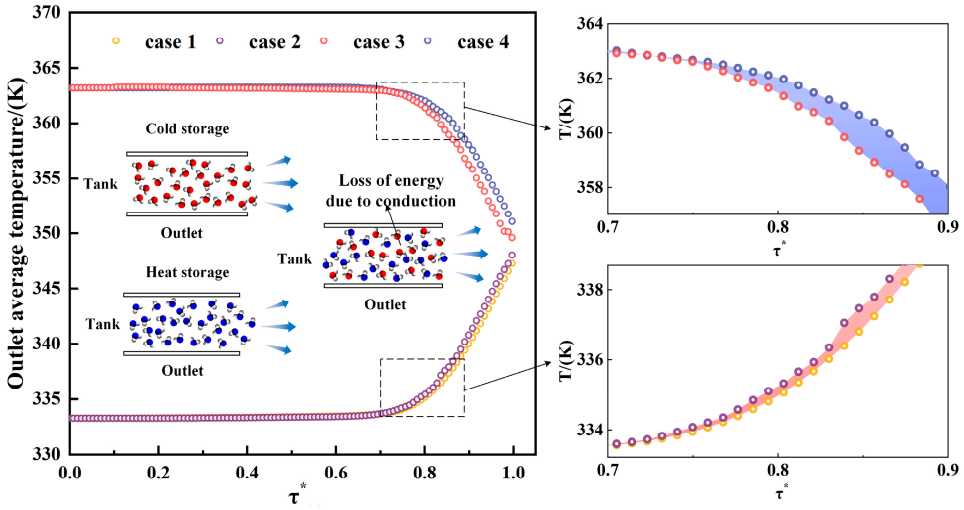


Figure 7. Changes in export temperature over time.

The dimensionless thickness of the thermocline and the efficiency of the energy storage process for various water distribution configurations are illustrated in Figure 8. During heat storage, the thermocline is thinner with an upward-facing upper water distributor, resulting in lower average wall temperatures compared to a downward-facing distributor. This configuration reduces heat dissipation and axial heat transfer losses, improving storage efficiency by approximately 0.45%. During cold storage, a downward-facing lower water distributor results in a thinner thermocline and lower average wall temperatures compared to an upward-facing distributor. Although heat dissipation is reduced, the decrease in mixing losses enhances cold storage efficiency by approximately 1.9%. In both heat and cold storage processes, thermal conductivity between hot and cold fluids causes the thermocline thickness to increase over time. Therefore, to enhance energy storage efficiency, the upper water distributor should be oriented upward, and the lower water distributor should be oriented downward.

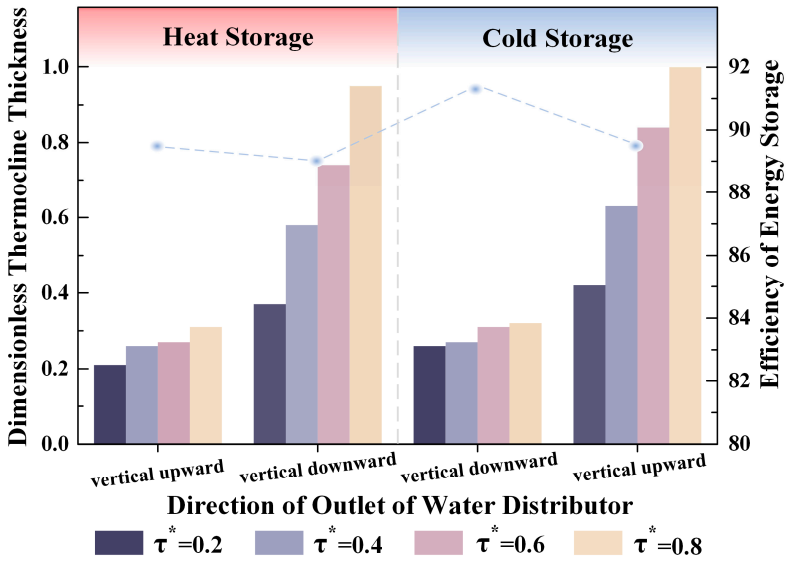


Figure 8. The variation of thermocline dimensionless thickness with time and energy storage efficiency at the end of thermal storage.

3.2. Influence of Water Distributor Construction on the Effectiveness of Heat Storage

The actual energy storage process using the water distributor involves a symmetrical structure, where hot and cold water enters the tank through branch pipes and distribution holes. As the number of distribution holes increases, the flow conditions within the distributor become more complex, leading to greater differences in exit flow rates. Therefore, the main inlet of the water distributor is designed to account for the differences in flow rates between various outlets, ensuring a distribution that better aligns with actual conditions.

The simulations of heat storage in the energy storage tank using star-type, antenna-type, and octagonal-type water distribution systems (hereinafter referred to as A, B, and C types) are designated as Case 5, Case 6, and Case 7, respectively. Except for the outlet configurations, the other simulation conditions are identical to those of Cases 1 through 4. The upper water distribution outlet is oriented upward, while the lower water distribution outlet is oriented downward. When the number of outlets, hole diameter, and outlet flow velocity of the distributor remain unchanged, both the Reynolds number and the Froude number are the same. Therefore, the only parameter affecting the distribution of storage efficiency under different operating conditions is the structural impact of the distributor itself. The three water distributor structures are axisymmetric, each featuring two axes of symmetry. The first axis, located at the branch, is designated as Line 1, with its corresponding axial surface referred to as Plane 1. The second axis, which is the axis of symmetry between two neighboring branches, is designated as Line 2, with its corresponding axial surface referred to as Plane 2. Figure 9 illustrates the temperature evolution of Plane 1 and Plane 2 under various operational conditions.

It is evident from Figure 10 that the trend of energy storage efficiency is affected by the evolution of the thermocline in the tank. Based on the evolution of the thermocline and the change in energy storage efficiency, the energy storage process can be divided into three phases: the initial phase, the transition phase, and the development phase.

In the initial phase (τ^* = 0~0.2), hot water enters the tank and mixes with the colder water near the outlet, resulting in partial energy loss. However, a thermocline gradually forms, which reduces the mixing of hot and cold water. This leads to a rapid increase in energy storage efficiency, as the thermocline mitigates further mixing. Both the mixing and thermocline formation impact efficiency changes during this stage.

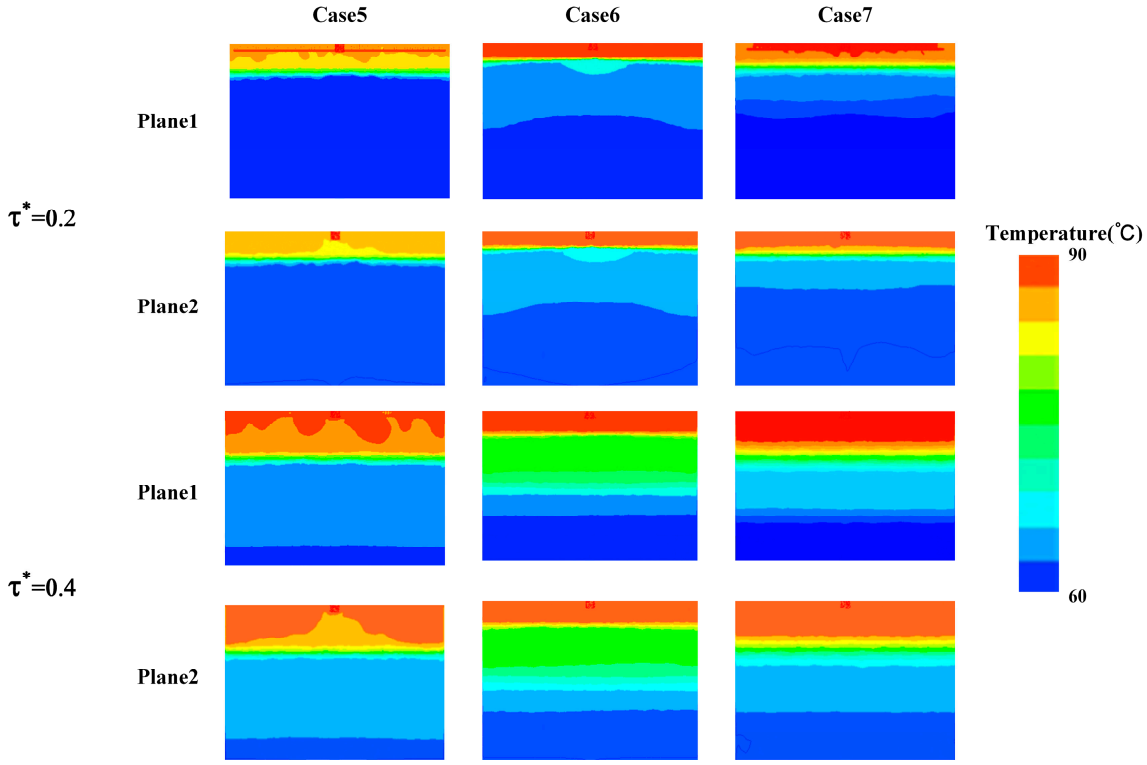


Figure 9. Temperature distribution on different planes changes over time.

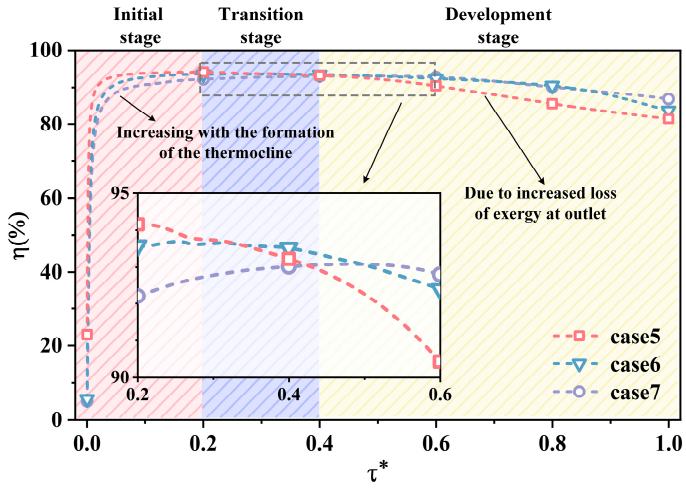


Figure 10. The change curve of energy storage efficiency with time in the energy storage process.

In the transition stage (τ^* = 0.2~0.4), the injected hot water creates a high-temperature zone in the upper part of the tank, resulting in a distinct thermocline between the colder water at the lower part. The hot water entering the inner part of the tank mixes predominantly with the existing high-temperature water, and this mixing is confined to the boundary of the thermocline. Consequently, the thermal losses are minimized, and the variation in storage efficiency remains relatively small during this phase. Moreover, changes in the thermocline will influence the subsequent variations in energy storage efficiency.

In the development stage (τ^* = 0.4~1), as the lower boundary of the inclined thermocline extends toward the tank's bottom, a portion of the heat is carried away with the outgoing cold water, initiating a reduction in energy storage efficiency across various operating conditions.

In the initial stage, the flow distribution of the water distributor determines the formation of the thermocline, which significantly impacts the energy storage efficiency. As shown in Figure 11, during heat storage, the average flow rate of hot water is highest at the inlet section of the branch pipe. As it passes through the distribution holes, the hot water enters the tank under pressure. According to the continuity equation and Bernoulli's principle, a decrease in flow rate through the distribution holes results in a lower average flow rate and an increase in pressure in the branch pipe. In the A-type distribution, where water distribution holes are located in the main branch, flow loss is significant. In contrast, the B and C-type distributions, with holes in the sub-branches, experience less flow loss, leading to more stable flow conditions. As shown in Figure 12, the velocity along the center line of the A-type distribution branch decreases radially. In the B and C-type distributions, the flow rate along the center line decreases in a "step" manner.

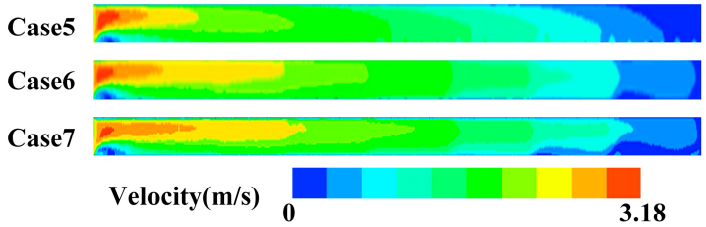


Figure 11. The flow rate distribution on the axial surface of the main branch of the water distributor with different structures.

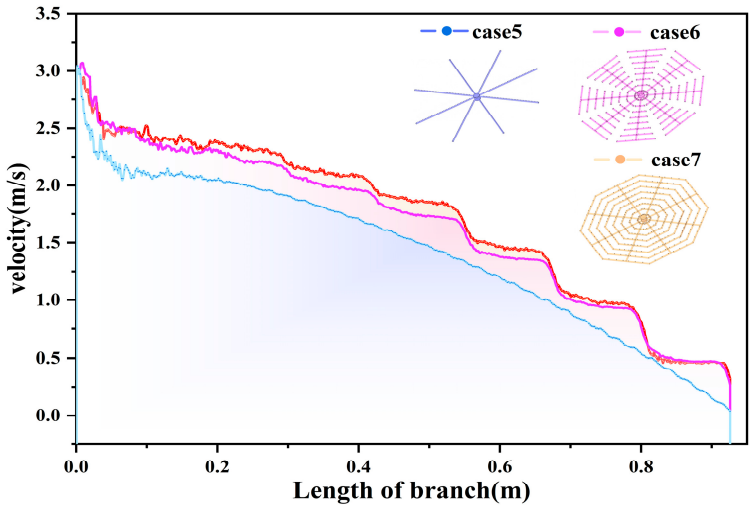


Figure 12. The distribution of the flow rate on the centerline of the main branch of the water distributor with different structures.

According to Figure 13, the tank volume is divided into eight regions, each exhibiting different flow distribution structures as shown in Figure 14. The water distributor is equipped with a distribution chamber in the center. In Region 1, the number of water distribution holes is small, resulting in a lower average volume flow rate. Consequently, the flow distribution in this region is much lower compared to other regions. The type A water distributor uses uniformly distributed water distribution holes along the branches. Except for Region 8, flow distribution in Regions 2–6 is relatively uniform. However, as the regions approach the tank walls, their area increases and more heat is required. The increased distance of water distribution holes from the center reduces thermal conductivity efficiency, leading to uneven temperature distribution in the radial plane of the energy storage tank. Water distributors B and C increase the number of water distribution holes

along the branch direction and incorporate bypass branches. This design improves the heat distribution within the regions, enhances the uniformity of heat source distribution in the axial plane of the energy storage tank, and reduces the thickness of the thermocline.

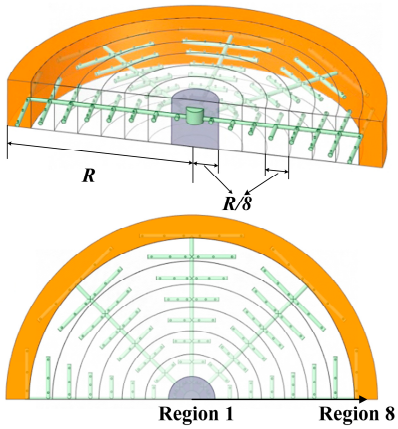


Figure 13. Division of tank area and region name.

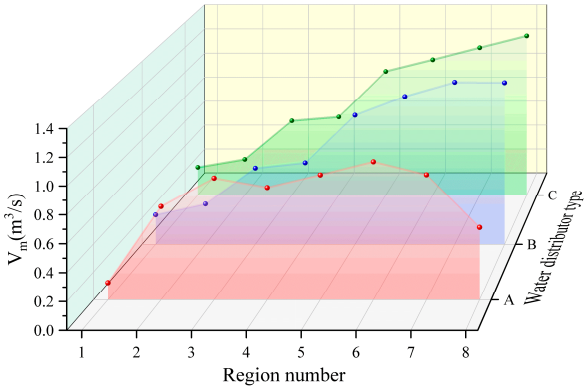


Figure 14. Flow distribution of different structures in different regions.

Figure 15, in Case 6 and Case 7, the temperature distribution on Line 1 and Line 2 is similar, and the radial temperature fluctuations are minimal. This suggests that the radial temperature distribution is more uniform when employing B and C types of water distribution systems for heat storage. Conversely, the greater temperature fluctuations observed in Case 5 imply that axial heat transfer is more pronounced, leading to a more uneven radial temperature distribution. Furthermore, the A-type water distribution system performs noticeably worse compared to the B and C systems. This demonstrates that flow distribution is the primary factor influencing temperature uniformity during the formation of the thermocline. To enhance temperature uniformity in the axial plane, it is crucial to ensure that flow distribution is optimized across various areas.

From Figure 9, it is evident that the temperature distribution varies significantly across different axial surfaces due to the varying placement of water distribution holes. Therefore, studying the evolution of the thermocline alongside the average temperature distribution of horizontal surfaces at different heights, as shown in Figure 16, is more scientifically rigorous. Initially, the use of the A-type water distributor results in uneven temperature distribution with localized heat concentration, which accelerates axial heat transfer in the tank. Consequently, the average temperature in the lower part of the tank is higher compared to the other two conditions. This leads to an increase in wall temperature, enhanced heat dissipation, and an increase in the thickness of the sloped thermocline. In contrast, the B- and C-type water distributors create a more uniform

temperature distribution, reducing the thickness of the sloped thermocline and improving the layering within the tank. As heat accumulates, heat concentration shifts to the upper part of the tank, enhancing axial heat transfer and gradually increasing the thickness of the thermocline. Over time, the thermocline exhibits a general downward translation trend. The development stage (τ^* = 0.4~1) is the phase with the longest time duration during the thermal storage process. Unlike the first two stages, the trend of energy storage efficiency in this phase continues to decline. During this stage, as the energy injection into the high-temperature zone gradually increases, the position of the thermal stratification layer moves downward. At the same time, the thickness of the stratified layer increases with time, and the boundary of the stratified layer gradually reaches the bottom of the tank. The outlet temperature begins to change and increases over time, with some of the heat being discharged along with the mixed water. In Case 5, due to the uneven temperature distribution, the axial heat transfer increases, and the stratified layer becomes the thickest. In this phase, the average temperature at the bottom of the tank is the highest, and thus the heat loss is the greatest. In contrast, Case 6 and Case 7 have the same axial heat conduction efficiency, but in Case 7, the region near the outlet within the stratified layer has a lower average temperature, which reduces the energy loss at the outlet. This indicates that the distribution and location of the stratified layer, as well as the temperature gradient near the outlet, play critical roles in improving thermal storage efficiency and minimizing heat loss.

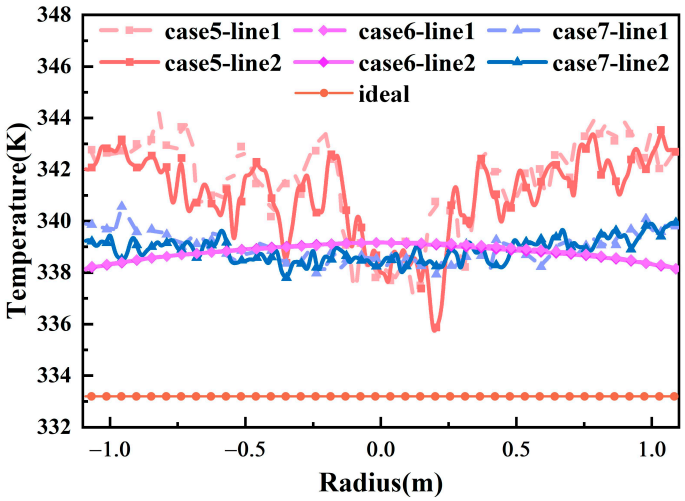


Figure 15. The temperature distribution on Line 1 and Line 2 at the tank height H = 1.2 m (τ^* = 0.2) for three different water distributor structures.

At the end of the transition stage (τ^* = 0.4), as the lower interface of the thermocline reaches the bottom of the tank, the outlet temperatures for Cases 5 and 6 begin to rise significantly. Concurrently, the expansion of the upper high-temperature zone causes a reduction in the volume of the thermocline that can be established, leading to a decrease in its thickness for all three conditions starting at τ^* = 0.6. As shown in Figure 17 During the period τ^* = 0.4~0.8, the outlet temperatures follow the order: Case 5 > Case 7 > Case 6. Case 5 experiences the highest heat loss due to the mixing of hot and cold water, whereas Case 6 exhibits the lowest heat loss. At τ^* = 0.8, the thickness of the thermocline in Case 6 increases, resulting in a rapid rise in the outlet temperature, as the temperature at the lower part of the thermocline in Case 6 is higher than that in Case 7.

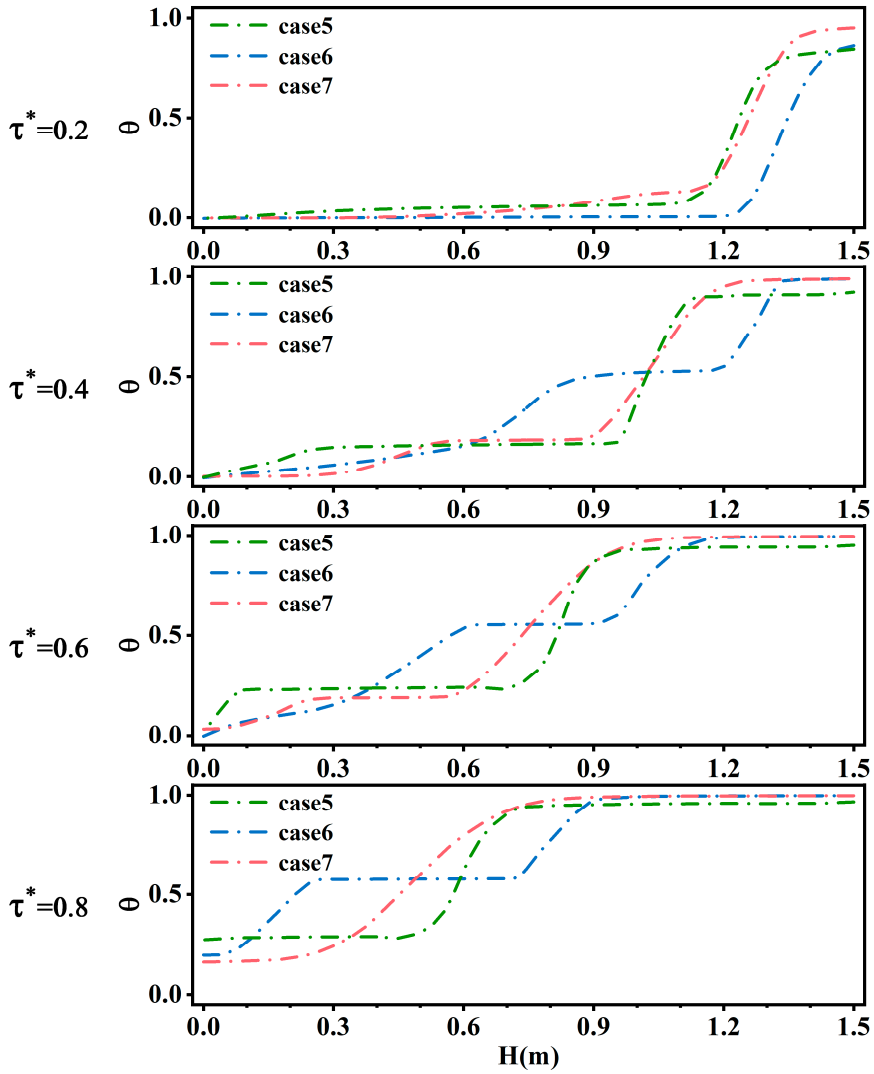


Figure 16. Average temperature distribution on the horizontal plane inside the tank.

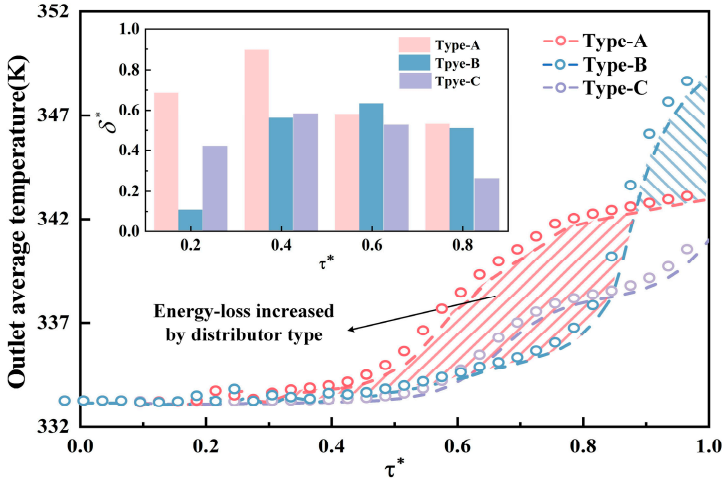


Figure 17. Changes in outlet temperature and thickness of the thermocline.

From Figure 18, at $\tau^* = 1$, the heat loss due to the mixing of hot and cold fluids is ranked as follows: Case 5 > Case 7 > Case 6. This ranking is primarily attributed to the differences in heat loss caused by fluid mixing, despite minimal variation in the average wall temperatures across different operating conditions. Case 7 exhibits the smallest heat

loss and achieves the highest thermal efficiency of 86.9%, which is 6.4% higher than that of Case 5. The difference in flow distribution due to the flow through the water distributor ultimately leads to a reduction in storage efficiency of about 8.3% compared to the ideal case where the flow rate at each outlet is the same.

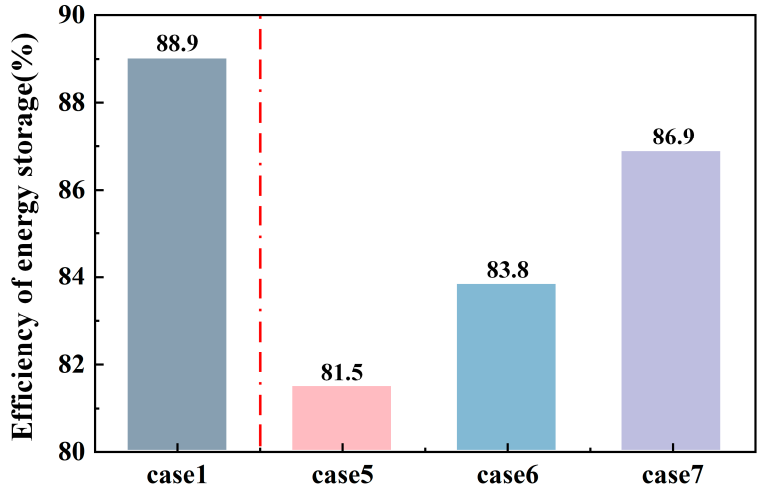


Figure 18. Efficiency at the end of energy storage with different structures.

4. Conclusions

The heat storage and release process in a cylindrical heat storage tank equipped with star-shaped water distributions was analyzed using numerical simulation methods. The study investigated how various installation directions of the water distribution influence the flow distribution within the tank. The degree of stratification was assessed based on parameters such as thermocline thickness, heat storage efficiency, and outlet temperature. The conclusions are summarized as follows:

(1) The fluid injected from the outlet of the water distributor exhibits inertia as it enters the tank, and when the outlet direction aligns with the movement direction of the naturally stratified fluid, it promotes the formation of the thermocline and enhances stratification. Thus, in the tank, the upper water distributor should be installed with the outlet facing upwards, and the lower water distributor should be installed with the outlet facing downwards.

(2) The energy storage process is divided into three stages based on changes in thermal storage efficiency. In the initial stage, the use of antenna-type and octagonal water distributors enhances the temperature uniformity of the axial surface, reduces the thickness of the thermocline, and improves the degree of stratification. At this stage, the final energy storage efficiency is primarily influenced by the energy losses resulting from the mixing of hot and cold water.

(3) In the development stage, the lower boundary of the thermocline reaches the exit position, leading to the exclusion of part of the hot water and a decrease in energy storage efficiency. Among the three structures, the designed octagonal water distribution exhibits the smallest energy loss and results in a 6.4% improvement compared to the star-type water distribution.

(4) When the star-type water distributor is installed in the storage tank, the resulting difference in flow distribution will lead to an 8.3% reduction in thermal storage efficiency compared to the ideal process.

The operating conditions in this study are based on a relatively high Reynolds number at the water distributor outlet, which holds significant research value for optimizing the performance of thermal storage tanks that are designed to complete large amounts of heat

storage within a short period. Considering the relatively large scale of the research model in this study, future experiments can utilize similarity criteria to establish a scaled-down model. By reducing the model's size, it would be possible to conduct more efficient and manageable experiments. Additionally, visual studies can be conducted to directly observe the development and evolution of the thermal stratification layer. Through these experiments, the stratified layer's formation, changes, and dynamics can be more intuitively demonstrated, providing valuable insights into improving the system's thermal storage efficiency and performance. This paper primarily focuses on the initial and development stages regarding the main factors influencing efficiency changes. However, the paper does not provide an in-depth investigation of the heat transfer and flow mechanisms during the second stage of thermocline evolution. Despite the significant impact of thermocline temperature distribution on subsequent stages, further investigation is warranted. Although the water distributor designed in this paper demonstrates some improvement in storage efficiency, its complex structure necessitates the exploration of more efficient and simplified designs. Consequently, developing a new, efficient, and simple water distributor structure remains essential for enhancing energy storage efficiency.

Author Contributions: X.W.: Methodology, Software, Validation, Formal analysis, Investigation, Data curation, Writing—original draft, Visualization. L.D.: Validation, Formal analysis, Investigation, Methodology, Software, Visualization. G.G.: Methodology, Supervision, Resources. W.Z.: Validation. D.S.: Supervision, Data curation. J.F.: Investigation, Validation. J.L.: Investigation, Writing—review and editing. R.L.: Writing—review and editing, Project administration. All authors have read and agreed to the published version of the manuscript.

Funding: This research was funded by the National Natural Science Foundation of China (52476143), and Youth Innovation Teams in Higher Education Institutions of Shandong Province (2023KJ064).

Data Availability Statement: The raw data supporting the conclusions of this article will be made available by the authors on request.

Conflicts of Interest: Author Genying Gao was employed by the Oil Production Technology Research Institute, China National Petroleum Corp. Xinjiang Oil Field. Authors Weibo Zheng and Dong Sun were employed by the Shengli Oilfield Technical Inspection Center, SlNOPEC. The remaining authors declare that the research was conducted in the absence of any commercial or financial relationships that could be construed as a potential conflict of interest.

References

1. Hoang, A.T.; Nguyen, X.P. Integrating renewable sources into energy system for smart city as a sagacious strategy towards clean and sustainable process. *J. Clean. Prod.* **2021**, *305*, 127161. [CrossRef]
2. Seferlis, P.; Varbanov, P.S.; Papadopoulos, A.I.; Chin, H.H.; Klemeš, J.J. Sustainable design, integration, and operation for energy high-performance process systems. *Energy* **2021**, *224*, 120158. [CrossRef]
3. Chang, C.; Xu, X.; Guo, X.; Rasakhodzhaev, B.; Zhao, M.; Yuan, G.J. Experimental and numerical study of ice storage and melting process of external melting ice coil. *J. Energy Storage* **2024**, *77*, 109961. [CrossRef]
4. Yang, S.; Nie, Z.; Wu, S.; Li, Z.; Wang, B.; Wu, W.; Chen, Z. A critical review of reservoir simulation applications in key thermal recovery processes: Lessons, opportunities, and challenges. *Energy* **2021**, *35*, 7387–7405. [CrossRef]
5. Wang, Y.; Han, X.; Li, J.; Liu, R.; Wang, Q.; Huang, C.; Wang, X.; Zhang, L.; Lin, R. Review on oil displacement technologies of enhanced oil recovery: State-of-the-art and outlook. *Energy Fuels* **2023**, *37*, 2539–2568. [CrossRef]
6. Mollah, M.B.; Zhao, J.; Niyato, D.; Lam, K.Y.; Zhang, X.; Ghias, A.M.; Koh, L.H.; Yang, L. Blockchain for future smart grid: A comprehensive survey. *IEEE Internet Things J.* **2020**, *8*, 18–43. [CrossRef]
7. Hossein Motlagh, N.; Mohammadrezaei, M.; Hunt, J.; Zakeri, B. Internet of Things (IoT) and the energy sector. *Energies* **2020**, *13*, 494. [CrossRef]
8. Njoku, H.; Ekechukwu, O.; Onyegegbu, S.O. Analysis of stratified thermal storage systems: An overview. *Heat Mass Transf.* **2014**, *50*, 1017–1030. [CrossRef]
9. Jebamalai, J.M.; Marlein, K.; Laverge, J. Influence of centralized and distributed thermal energy storage on district heating network design. *Energy* **2020**, *202*, 117689. [CrossRef]

10. Lou, W.; Xie, B.; Aubril, J.; Fan, Y.; Luo, L.; Arrivé, A. Optimized flow distributor for stabilized thermal stratification in a single-medium thermocline storage tank: A numerical and experimental study. *Energy* **2023**, *263*, 125709. [CrossRef]
11. Xie, B.; Baudin, N.; Soto, J.; Fan, Y.; Luo, L. Wall impact on efficiency of packed-bed thermocline thermal energy storage system. *Energy* **2022**, *247*, 123503. [CrossRef]
12. Gajbhiye, P.; Salunkhe, N.; Kedare, S.; Bose, M. Experimental investigation of single media thermocline storage with eccentrically mounted vertical porous flow distributor. *Sol. Energy* **2018**, *162*, 28–35. [CrossRef]
13. König-Haagen, A.; Höhlein, S.; Brüggemann, D. Detailed exergetic analysis of a packed bed thermal energy storage unit in combination with an Organic Rankine Cycle. *Appl. Therm. Eng.* **2020**, *165*, 114583. [CrossRef]
14. Yang, Z.; Chen, H.; Wang, L.; Sheng, Y.; Wang, Y. Comparative study of the influences of different water tank shapes on thermal energy storage capacity and thermal stratification. *Renew. Energy* **2016**, *85*, 31–44. [CrossRef]
15. Chen, J.; Xu, H.; Wang, Z.; Han, S. Thermal Performance Study of a Water Tank for a Solar System with a Fresnel Lens. *J. Sol. Energy Eng.* **2018**, *140*, 051005. [CrossRef]
16. Li, G. Sensible heat thermal storage energy and exergy performance evaluations. *Renew. Sustain. Energy Rev.* **2016**, *53*, 897–923. [CrossRef]
17. Ievers, S.; Lin, W. Numerical simulation of three-dimensional flow dynamics in a hot water storage tank. *Appl. Energy* **2009**, *86*, 2604–2614. [CrossRef]
18. Khurana, H.; Tiwari, S.; Majumdar, R.; Saha, S.K. Comparative evaluation of circular truncated-cone and paraboloid shapes for thermal energy storage tank based on thermal stratification performance. *J. Energy Storage* **2021**, *34*, 102191. [CrossRef]
19. Wang, Z.; Zhang, H.; Dou, B.; Huang, H.; Wu, W.; Wang, Z. Experimental and numerical research of thermal stratification with a novel inlet in a dynamic hot water storage tank. *Renew. Energy* **2017**, *111*, 353–371. [CrossRef]
20. Dragsted, J.; Furbo, S.; Dannemand, M.; Bava, F. Thermal stratification built up in hot water tank with different inlet stratifiers. *Sol. Energy* **2017**, *147*, 414–425. [CrossRef]
21. Rahman, A.; Smith, A.D.; Fumo, N. Performance modeling and parametric study of a stratified water thermal storage tank. *Appl. Therm. Eng.* **2016**, *100*, 668–679. [CrossRef]
22. Yaïci, W.; Ghorab, M.; Entchev, E.; Hayden, S. Three-dimensional unsteady CFD simulations of a thermal storage tank performance for optimum design. *Appl. Therm. Eng.* **2013**, *60*, 152–163. [CrossRef]
23. Nelson, J.; Balakrishnan, A.; Murthy, S.S. Experiments on stratified chilled-water tanks: Expériences menées avec des reservoirs d'accumulation d'eau glacée à stratification. *Int. J. Refrig.* **1999**, *22*, 216–234. [CrossRef]
24. Shaikh, W.; Wadegaonkar, A.; Kedare, S.; Bose, M. Numerical simulation of single media thermocline based storage system. *Sol. Energy* **2018**, *174*, 207–217. [CrossRef]
25. Advaith, S.; Parida, D.R.; Aswathi, K.T.; Dani, N.; Chetia, U.K.; Chattopadhyay, K.; Basu, S. Experimental investigation on single-medium stratified thermal energy storage system. *Renew. Energy* **2021**, *164*, 146–155. [CrossRef]
26. Xu, X.; Chang, C.; Dong, J.; Guo, X.; He, M.; Yu, Q. Analysis and optimization of thermal storage performance of single tank thermocline layer with built-in insulation board. *J. Energy Storage* **2024**, *97*, 112712. [CrossRef]
27. Gao, L.; Lu, H.; Sun, B.; Che, D.; Dong, L. Numerical and experimental investigation on thermal stratification characteristics affected by the baffle plate in thermal storage tank. *J. Energy Storage* **2021**, *34*, 102117. [CrossRef]
28. Karim, M. Experimental investigation of a stratified chilled-water thermal storage system. *Appl. Therm. Eng.* **2011**, *31*, 1853–1860. [CrossRef]
29. Hosseinnia, S.M.; Akbari, H.; Sorin, M. Numerical analysis of thermocline evolution during charging phase in a stratified thermal energy storage tank. *J. Energy Storage* **2021**, *40*, 102682. [CrossRef]
30. Chung, J.D.; Cho, S.H.; Tae, C.S.; Yoo, H. The effect of diffuser configuration on thermal stratification in a rectangular storage tank. *Renew. Energy* **2008**, *33*, 2236–2245. [CrossRef]
31. Tang, J.; OuYang, Z.; Shi, Y. Diffuser design and experimental research of a large-scale chilled water storage system. *Energy Sources Part A Recovery Util. Environ. Eff.* **2021**, *43*, 1456–1467. [CrossRef]

Disclaimer/Publisher's Note: The statements, opinions and data contained in all publications are solely those of the individual author(s) and contributor(s) and not of MDPI and/or the editor(s). MDPI and/or the editor(s) disclaim responsibility for any injury to people or property resulting from any ideas, methods, instructions or products referred to in the content.